Quantum Sensing and Information Processing

Lecture 3: Sensing with Quantum Devices

June 27th, 2019

Stephen B. Libby
David H. Chambers

LLNL-PRES-780497
This work was performed under the auspices of the U.S. Department of Energy by Lawrence Livermore National Laboratory under contract DE-AC52-07NA27344. Lawrence Livermore National Security, LLC

Lawrence Livermore National Laboratory

Lecture Schedule Update

Control of Quantum Devices --- Lisa Poyneer

~~Tuesday, July 2nd at 2:00, B132S R1000, GS/WCI Auditorium~~

Error Modelling — Steve Libby

Tuesday, July 9th at 2:00, B543 Auditorium, R1001

Application: Quantum Computation — Jonathan Dubois

Tuesday, July 23th at 2:00, B543 Auditorium, R1001

Application: Quantum Computing Algorithms — Andreas Baertschi (LANL)

Wednesday, July 31st at 2:00, B543 Auditorium, R1001

Thursday, August 1st at 2:00, B543 Auditorium, R1001

Application: Quantum Radar — Matthew Horsley

Tuesday, August 13th at 2:00, B543 Auditorium, R1001

Schedule posted to Lab calendar – subscribe to receive updates

https://casis.llnl.gov/seminars/quantum_information

Quantum Coherent Control is Driving Significant Advances in Precision Sensing & Measurement

- Quantum Sensor advantages: great precision, environmental control and isolation, intrinsic 'self-calibration,' 'instant on,' no significant baseline drift – natural for fast, real time applications.

- Synergistic with quantum computing. Exploit multi-qubit gates protocols (Hadamard/Pauli vs. $\pi/2$ & π pulses)

- Applications: atomic clocks, field and force sensors (e.g., gravity, inertial navigation, magnetism), metrology, fundamental science (e.g. axions, dark matter, gravitational waves,…)

- Atomic fountain and Sagnac interferometry (exploits quantum correlated internal atomic and momentum states).
  - *Gravity gradiometry* (mass 'tomography')
    - Hidden mass detection at close range (portal scan & emergency response) – (current LLNL/AOSense)
    - Further applications: tunnel/underground structure detection, city scan, treaty verification, naval.
  - *Inertial motion sensors* – beyond GPS – dead reckoning navigation (current AOSense/LLNL)

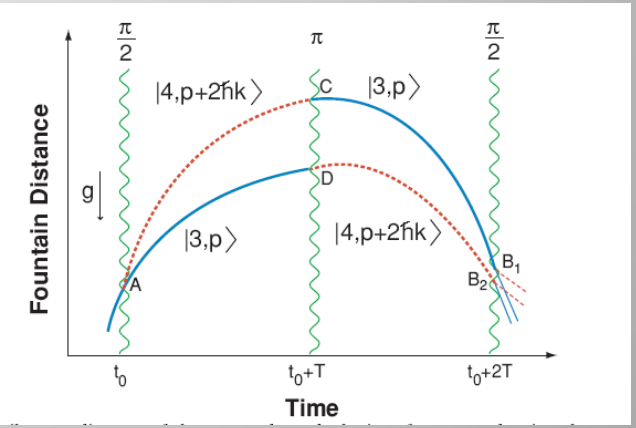

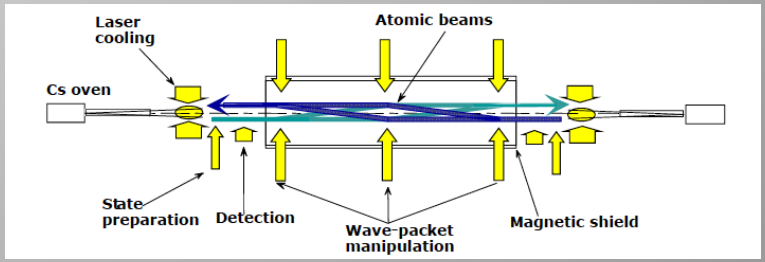

The LLNL/AOSense Cold Atom Gravity & Gyro Sensor Team

LLNL:

- Stephen Libby
- David Chambers
- Hema Chandrasekharan
- Vijay Sonnad
- Steven Kreek
- Karl Nelson
- Mark Cunningham
- Lance Bentley Tammero
- Kristin Lennox
- Steven Bond
- Jake Trueblood
- John Taylor, Pete Davis, Stan Edson, Pete Fitsos
- Kyle Brady (UC Berkeley – summer student 2010)
- Rees McNally (U. Colorado – summer student 2013)
- Ming-Yee Tsang (Princeton – summer student 2014)
- Samuel Stone (Cal State Chico – summer student 2017)

AOSense, Inc.:

- Brenton Young
- Miro Shverdin
- Mike Matthews
- Matt Cashen
- Boris Dubetsky
- Alan Zorn
- Adam Black
- Mark Kasevich
- Jamil Abo-Shaeer
- Tom Loftus

Quantum Sensing: Detection, Interferometry, Noise* - *Requirements*!

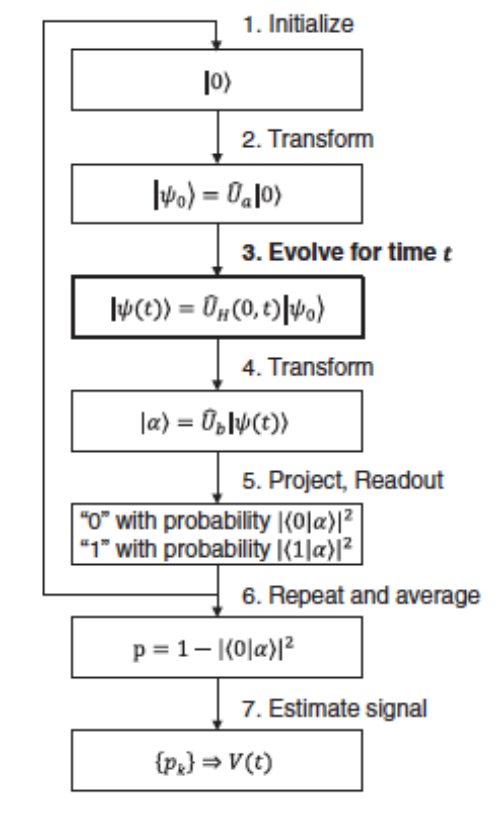

Basic steps in the quantum sensing process

How does quantum noise limited sensitivity drive our 'quantum device' design?

Atomic fountain clock & cold atom interferometry examples

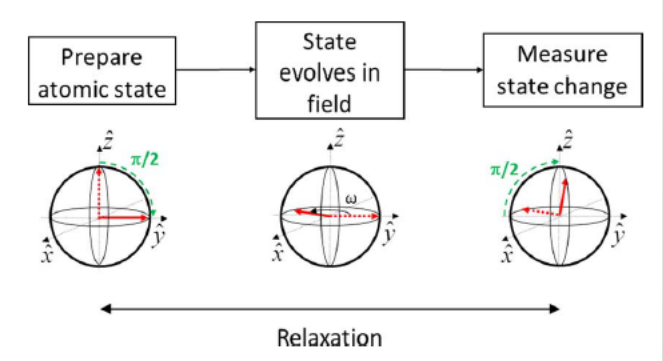

Ramsey Interferometry

$$|\psi_0\rangle = |+\rangle \equiv \frac{1}{\sqrt{2}}(|0\rangle + |1\rangle) \Rightarrow |\psi(t)\rangle = \frac{1}{\sqrt{2}}(|0\rangle + e^{-i\omega_0 t}|1\rangle) \Rightarrow |\alpha\rangle = \tfrac{1}{2}(1 + e^{-i\omega_0 t})|0\rangle + \tfrac{1}{2}(1 - e^{-i\omega_0 t})|1\rangle$$

$$p = 1 - |\langle 0|\alpha\rangle|^2 = \sin^2(\omega_0 t/2) = \tfrac{1}{2}[1 - \cos(\omega_0 t)]$$

Quantum Projection Noise Limited Sensitivity

$$\delta F_{\min} = \frac{h\delta\varphi}{\mu T} \qquad \delta F_{\min} = \frac{h\delta\varphi}{\mu T_2}\sqrt{\frac{T_2}{T}} = \frac{h}{\mu\sqrt{T_2 T N}}$$

**Quantum sensing*, C. L. Degen, F. Reinhard, P. Cappellaro, RMP, 89, 035002, (2017).

Atomic Sensors – a review, J. Kitching, S. Knappe, E. A. Donley, IEEE Sensors, 11, 9, 1749, (2011).

Squeezed atomic states and projection noise in spectroscopy, D. J. Wineland, J. J. Bollinger, W. M. Itano, and D. J. Heinzen, Phys. Rev. A, vol. 50, pp. 67–88, (1994).

First Observation of Gravitationally Induced Quantum Interference*

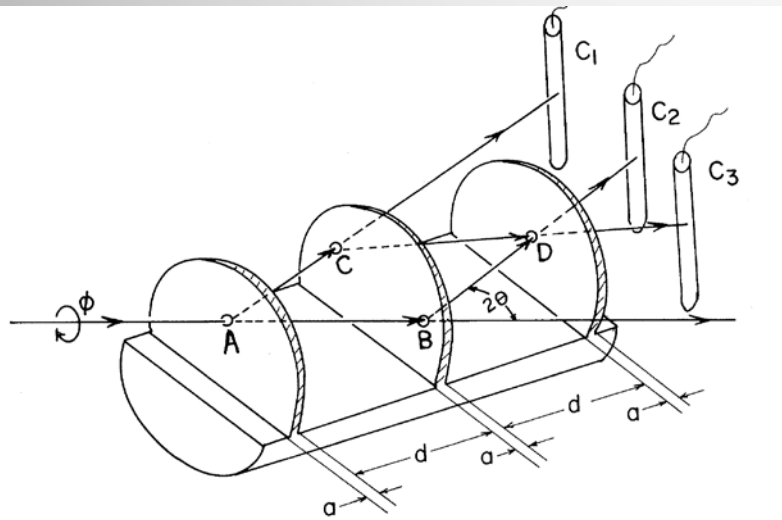

FIG. 1. Schematic diagram of the neutron interferometer and ^{3}He detectors used in this experiment.

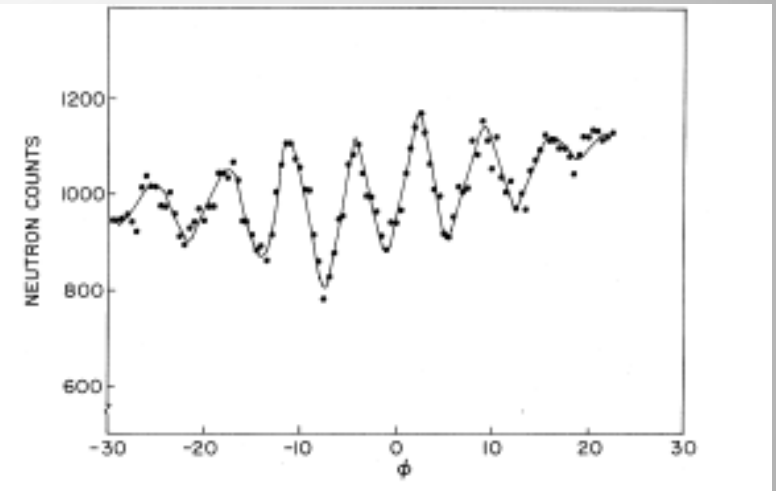

$$\Delta\varphi = s\Delta k$$

$$\Delta k \cong M^2 g r \lambda / h^2$$

- Neutron de Broglie wavelength ~ 1.445 Å
- Neutron velocity ~ 10^3 m/sec.

* R. Colella, A. W. Overhauser, and S. A. Werner, Observation of Gravitationally Induced Quantum Interference, Phys. Rev. Lett. 34, 1472, (1975).

Atomic fountain clock

- Atomic clocks use Ramsey split field interferometry in various modes.
- Zacharias's 1950's atomic fountain idea finally implemented after the discovery of laser cooling – fountain greatly increases the microwave interrogation time.
- Sequential $\frac{\pi}{2}$ pulses in waveguide.
- Central Ramsey fringe < 1 Hz (for Cesium 9 GHz hyperfine)
- 50,000 sec averaging/servo feedback.
- Enabled clocks (e. g. NIST FS-2) with accuracy better than 10^{16}

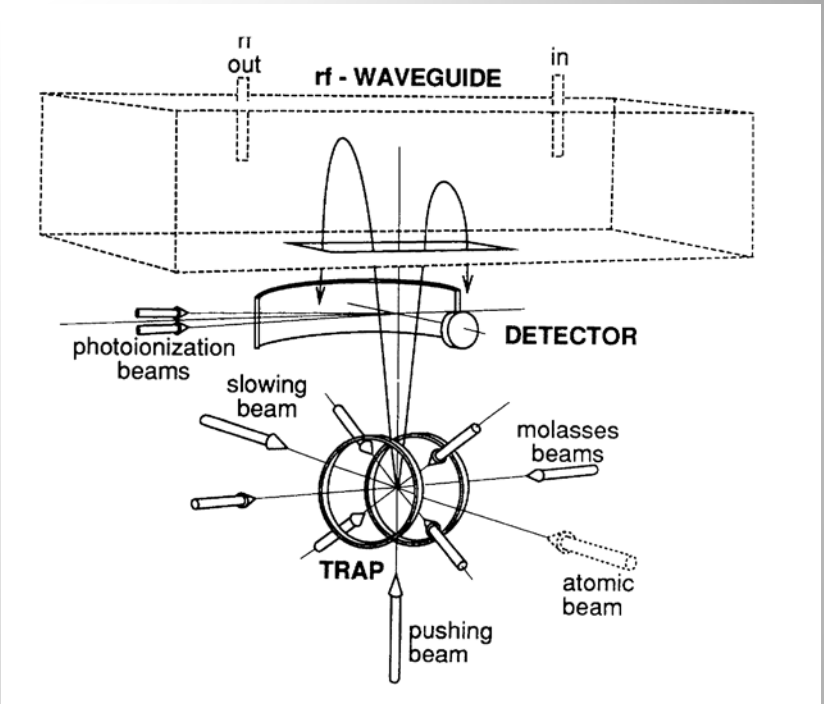

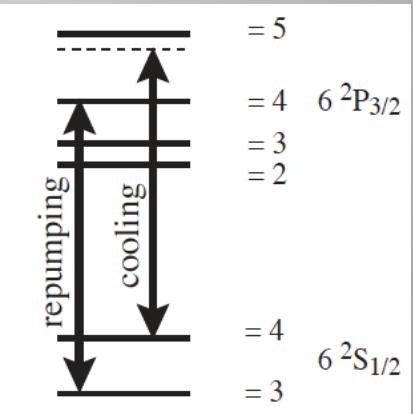

J. L. Hall, M. Zhu, and P. Buch, *Prospects for using laser-prepared atomic fountains for optical frequency standards applications*, JOSA B, Vol. 6, # 11, pp. 2194-2205 (1989)

M. A. Kasevich, E. Riis, and S. Chu, R. G. DeVoe, *RF Spectroscopy in an Atomic Fountain*, 63, # 6 Phys. Rev. Lett. (1989), 612

Designing an atom interferometer for inertial sensing: atomic fountain clock & optically stimulated Raman to separate the wavepacket

Resonant optical interaction

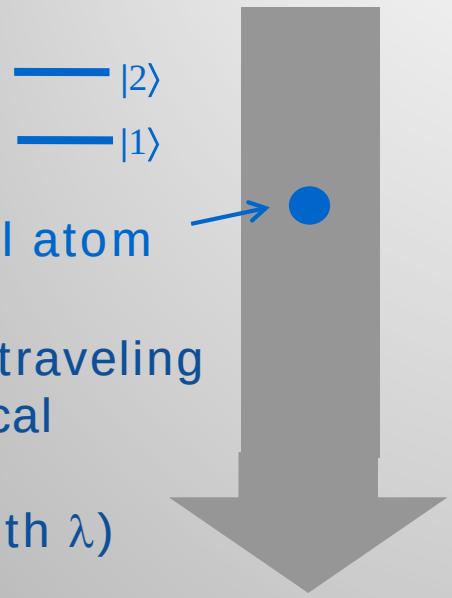

$$|\psi(t)\rangle = \cos\left(\frac{\Omega t}{2}\right)|1,\mathbf{p}\rangle + e^{-i\frac{\pi}{2}} e^{i\phi_L} \sin\left(\frac{\Omega t}{2}\right)|2,\mathbf{p}+\hbar\mathbf{k}_{\mathrm{eff}}\rangle$$

Recoil diagram

- Momentum conservation between atom and laser light field (recoil) leads to spatial separation of atomic wavepackets.

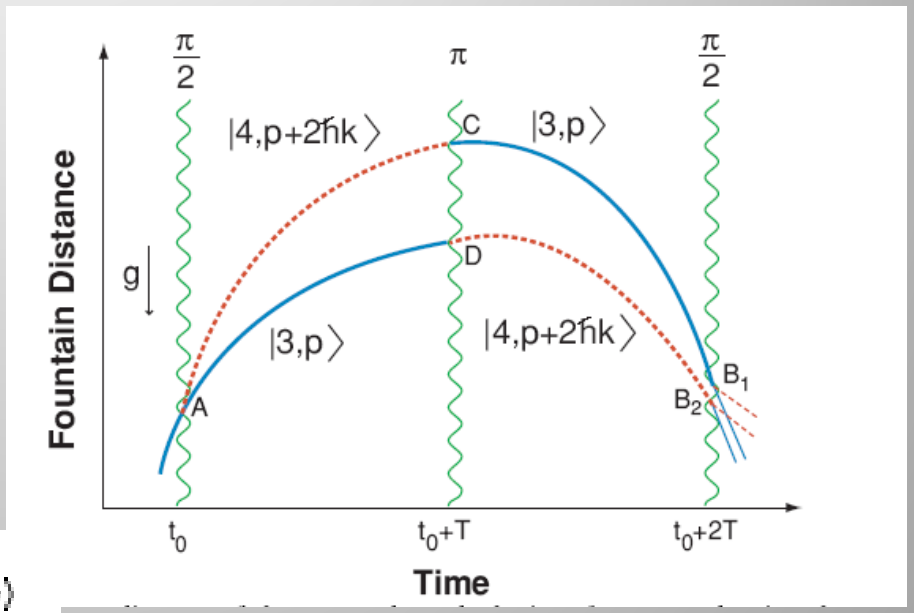

- 780 nm laser stabilized to < 1 kHz can measure the atom's position ~ 1:10^{12} .

Atomic deflection due to 25 kg mass at a distance of 1 meter over Δt ~ .25 sec is ~.5 Å.

- Semi-classical phase shift ~ $n\hbar k\delta g T^2$ High momentum transfer n >> 2.

Optically stimulated Raman transitions – Rabi oscillations between hyperfine states - advantages for quantum interferometry!

Level scheme

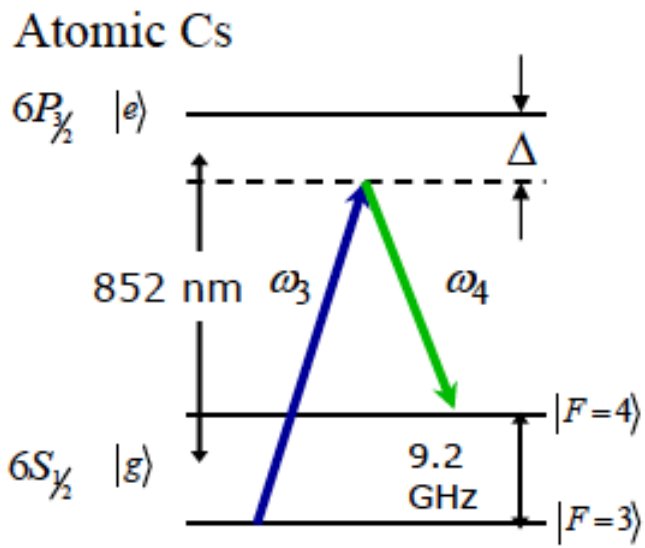

Excitation Geometry

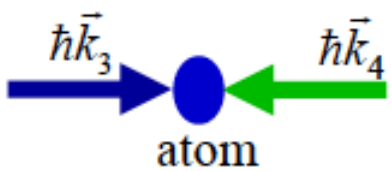

Doppler sensitive configuration

- $\mathbf{k}_3$, $\mathbf{k}_4$ counter-propagate

Ground states

- Avoid spontaneous emission
- Excitation between magnetic field insensitive sublevels

Large detuning D

- Effective 2-level system

  $F=3, m_f=0 \leftrightarrow F=4, m_f=0$

- Effective traveling wave excitation

  $\mathbf{k}_{eff} = \mathbf{k}_3 - \mathbf{k}_4 \sim 2\mathbf{k}_3$

- Effective transition frequency

  $\Delta\omega_{eff} = \omega_3 - \omega_4$

The atomic fountain interferometer is making a stroboscopic movie of falling atoms

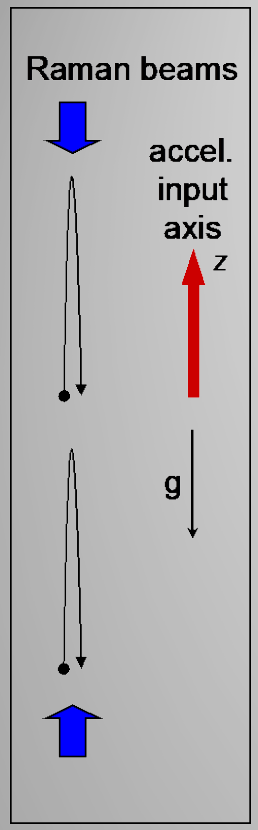

Paired atom fountains 'interrogated' by common Raman lasers – PINS gradiometer

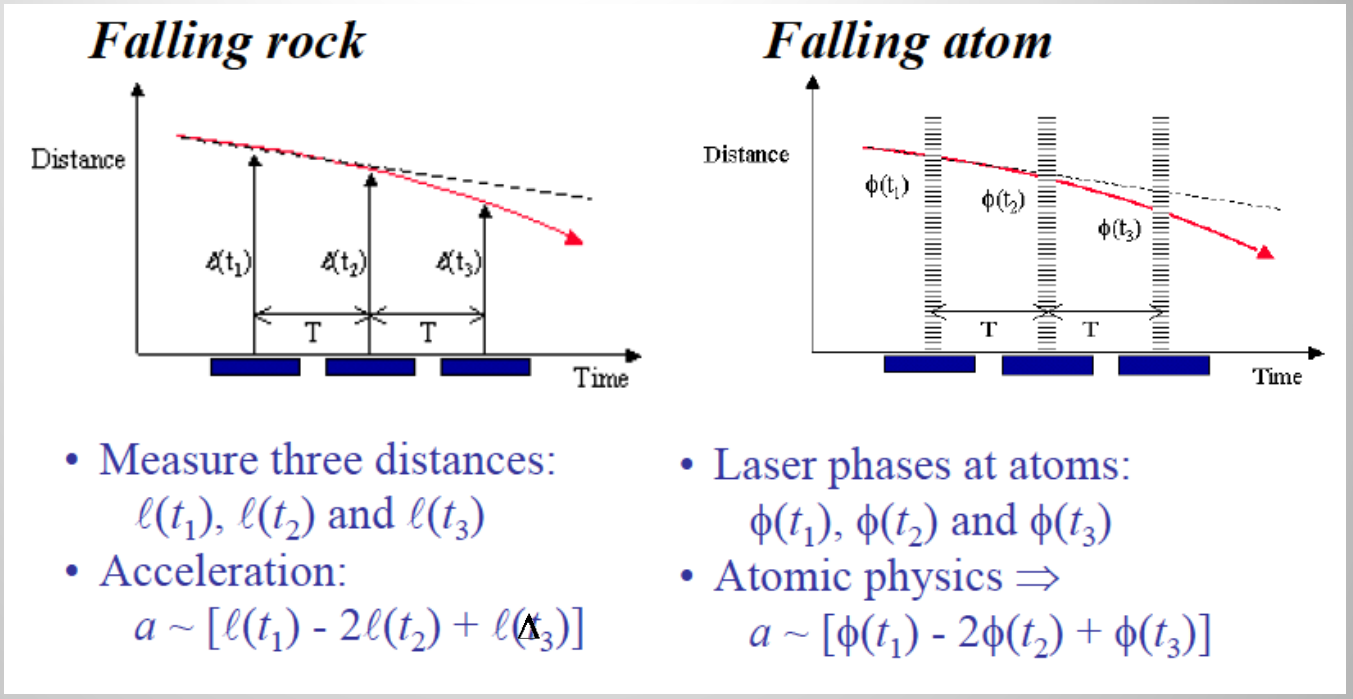

Gravity gradient is $T_{zz} = (g_1-g_2)/L$. 1 Eötvös is 10^{-9} s^{-2}. Gravity gradient of Earth at Earth surface is 3 10^{-6} s^{-2}.

Gravity gradient of 25 kg sphere at 1 meter is 3.4 10^{-9} s^{-2}.

GG directly above 1.5 x 1.5 m^2 tunnel buried 30 m ~ .8 10^{-9} s^{-2}.

Individual interferometer gross phase ~ $k_{eff}\, gT^2$ ~ 10^8 radians (due mainly to the earth). Shot noise limited phase sensitivity ~ $1/\sqrt{N_{pulse}}$ ~ 10^{-3} rad.

Cold-Atom interferometry gravity sensors demonstrate off-the-chart performance

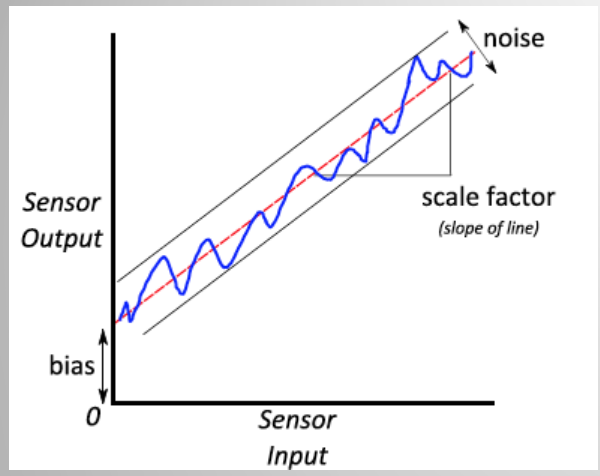

AI sensor performance in open literature:

- Bias stability: <<10^{-10} g
- Noise: < 4×10^{-9} g/Hz$^{1/2}$
- Scale Factor: < 10^{-10}

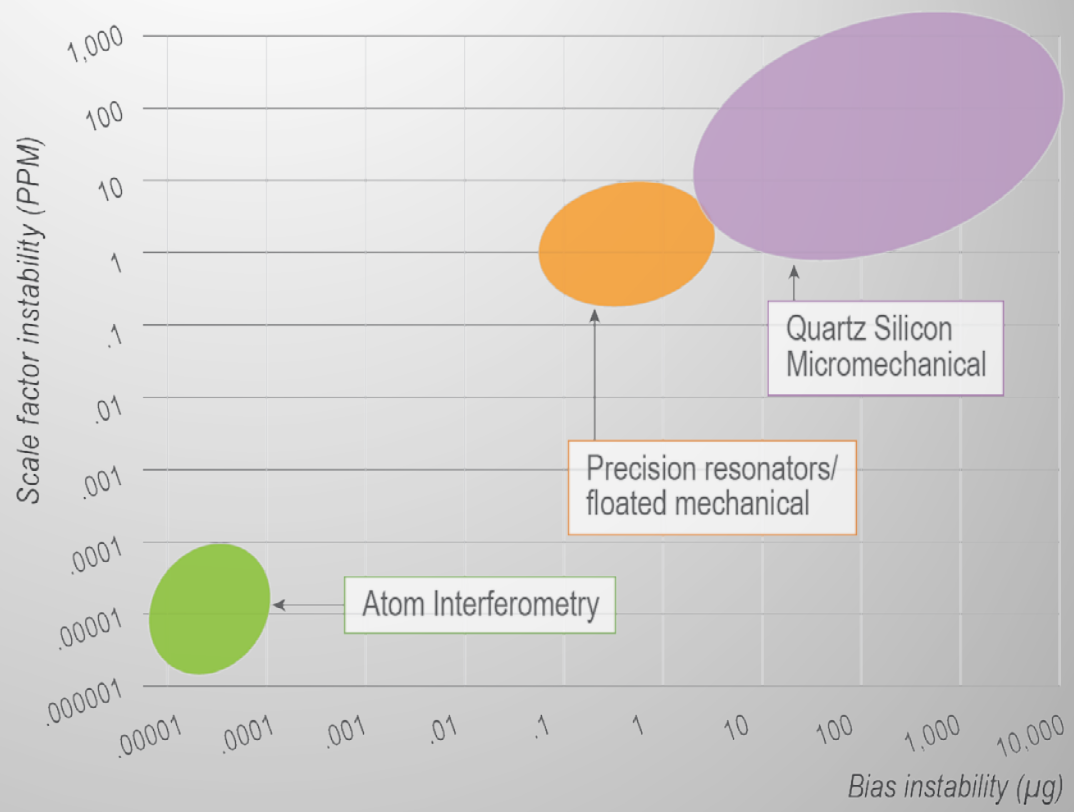

Quantum projection noise limited performance (present) depends on *D, T,* number of atoms *N*, photon recoil k_{eff}, interference fringe contrast η:

$$\Delta T_{zz} \approx \frac{1}{\eta\sqrt{N}\, D\, k_{eff} T^2}$$

Squeezed state detection ~ $1/N^q$ (.5 < q < 1). Uncertainty limit ~ 1/N

Two Photon Raman Atomic Fountain Interferometer – Semi-classical Gravitational Phase Shift Analysis & Gradiometer Response

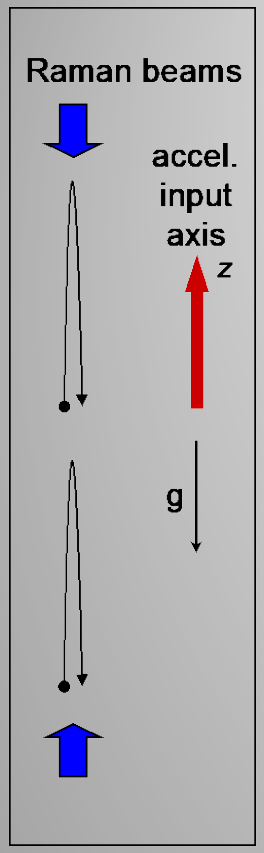

Paired atom fountains 'interrogated' by common Raman lasers

- Cold cesium atoms at ~ 1 μK (v ~ 1 cm/sec)
- Cooled, (initially F=3) cloud of ~ 10^8 alkali atoms. Unperturbed launch trajectory: v_0~ 2- 3 m/sec. t_1= 45 ms. T~ 250 ms. z_{02}- z_{01} ~ .5 m
- Raman laser wavevector k_{eff} ~ 10^7 m^{-1}.
- Semiclassical treatment: Mach-Zehnder steps are in 'sudden' approximation. $O(T^2)$ phase shift is solely due to light-atom interaction (k.δx) (higher order has Coriolis cross couplings, etc.)
- Individual interferometer gross phase ~ k_{eff} gT^2 ~ 10^8 radians (due mainly to the earth).
- Interferometer differences $\delta\varphi^{(1)}$-$\delta\varphi^{(2)}$: 1 to 10^{-4} rad. (10^{-3} rad ~ 2 10^{-9} /sec^2). Shot noise limited.
- Quantum corrections computed.

$$\phi_{tm} = \vec{k}_{eff}\,\delta\vec{\phi},$$
$$\delta\vec{\phi} = \delta\vec{x}(t_1+2T) - 2\delta\vec{x}(t_1+T) + \delta\vec{x}(t_1)$$

$$\delta\vec{x}(t) = \int_0^t dt'\,(t-t')\,\delta\vec{g}\left[\vec{x}_0(t')\right]$$

$$r(x) = \frac{\delta\phi_z^{(2)} - \delta\phi_z^{(1)}}{T^2(z_{02}-z_{01})}$$

Gravity gradiometer – the beginnings of mass tomography (2010)*
LLNL/AOSense collaboration

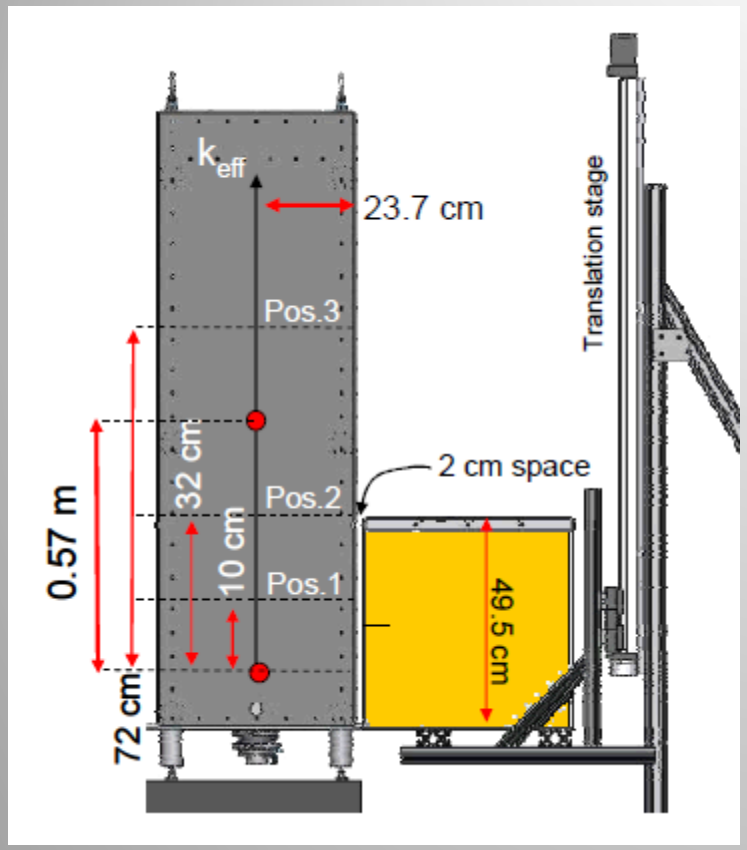

Sample mass configurations:

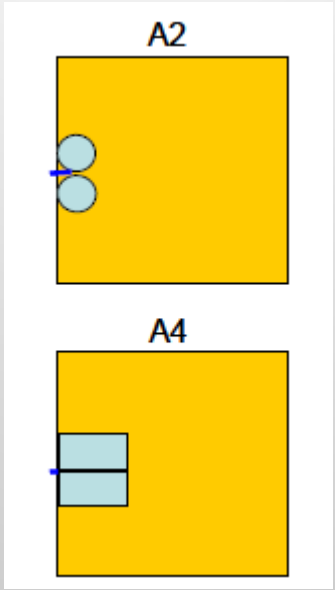

Data:

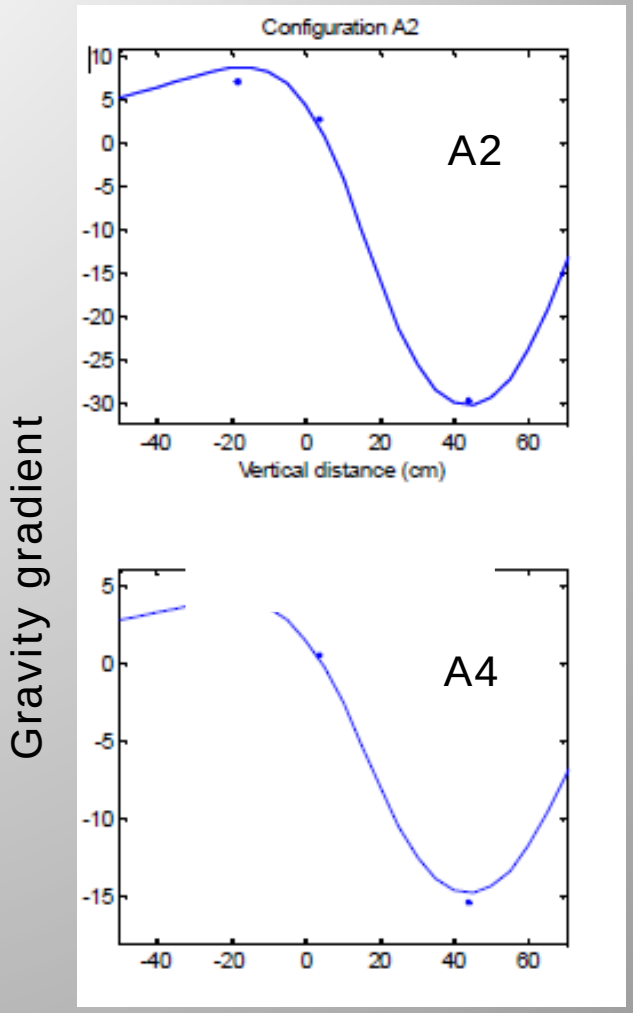

*"*Feasibility Study of a Passive, Stand-off Detector of High-Density Masses with a Gravity Gradiometer Based on Atomic Interferometry*," S. B. Libby, P.I., LLNL LDRD, FY 2010.

The atom interferometer gravimeter has the potential to measure subtle relativistic and geological effects

- Parametrized Post Newtonian treatment of the sensor response to the Earth's field. Use action to determine quantum phase – Dimopoulos, et. al., PRD 78, 2008.

$$\phi_{\text{propagation}} = \int L dt = \int m d\tau = \int p_\mu dx^\mu,$$

$$ds^2 = (1+2\phi)dt^2 - \frac{1}{1+2\phi}dr^2 - r^2 d\Omega^2$$

- Schwarzchild model of earth's field

- Effective acceleration form:

$$\frac{d\vec{v}}{dt} = -\vec{\nabla}(\phi + (\beta+\gamma)\phi^2) + \gamma(3(\vec{v}\cdot\hat{r})^2 - 2\vec{v}^2)\vec{\nabla}\phi + 2\vec{v}(\vec{v}\cdot\vec{\nabla}\phi)$$

	GR phase shift	Size (rad)	Interpretation
1.	$-k_{\text{eff}} g T^2$	3×10^8	Newtonian gravity
2.	$-k_{\text{eff}}(\partial_r g) v_L T^3$	-2×10^3	1st gradient
3.	$-\frac{7}{12}k_{\text{eff}}(\partial_r g)T^4$	9×10^2	
4.	$-3k_{\text{eff}} g^2 T^3$	-4×10^1	finite speed of light and
5.	$-3k_{\text{eff}} g v_L T^2$	4×10^1	Doppler shift corrections
6.	$-\frac{k_{\text{eff}}^2}{2m}(\partial_r g)T^3$	-7×10^{-1}	1st gradient recoil
7.	$(\omega_{\text{eff}} - \omega_a) g T^2$	-4×10^{-1}	detuning
8.	$(2-2\beta-\gamma)k_{\text{eff}} g \phi T^2$	-2×10^{-1}	GR (nonlinearity)
9.	$-\frac{3k_{\text{eff}}^2}{2m} g T^2$	2×10^{-2}	
10.	$-\frac{7}{12}k_{\text{eff}}(\partial^2 g)T^4$	8×10^{-3}	2nd gradient

- Curvature measurement – Asenbaum et. al. PRL, 2016.

- MAGIS 100 – gravitational radiation .1 – 1 Hz, dark matter detection, GR tests

- Clocks with uncertainties < 10^{-17} capable of redshift determinations of geodesic height - Mehlstaubler et. al., *Atomic clocks for geodesy*, Rep. Prog. Phys 81, (2018), 064401.

$$\frac{\Delta\nu}{\nu} \sim \frac{-gH}{c^2}$$

H is about 10 cm for $\frac{\Delta\nu}{\nu} \sim 10^{-17}$

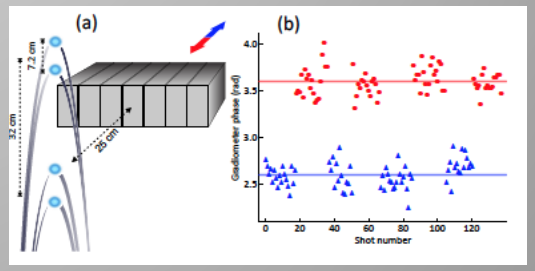

Gravity kernel is highly ill posed! –Singular Value Decomposition

- The singular behavior of the gravity kernel leads to the application of probabilistic likelihood (e.g. WINOVA – D. Chambers talk) or regularization methods (e.g. Tikhonov) driven by prior knowledge (hypotheses).

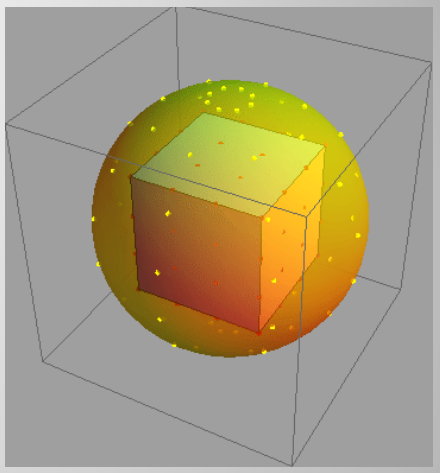

- Since our gravity kernel is ultimately a linear functional over the potentials we can usefully study the singular value behaviors of the matrix describing the potentials at exterior points r_j due to masses (m_i) at r_i.

$$\begin{pmatrix} \varphi_1 \\ \varphi_2 \\ \vdots \end{pmatrix} = \begin{pmatrix} \frac{1}{r_{11}} & \frac{1}{r_{12}} & \cdots \\ \frac{1}{r_{21}} & \frac{1}{r_{22}} & \cdots \\ \vdots & \vdots & \ddots \end{pmatrix} \begin{pmatrix} m_1 \\ m_2 \\ \vdots \end{pmatrix}$$

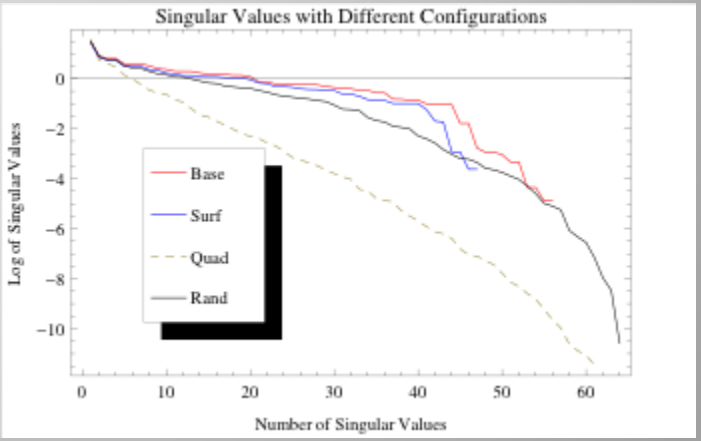

- For the example illustrated at the right, with the potentials measured on a sphere outside a variety of cubic mass distributions, we find that the matrix problem is highly ill posed (with the exception of 'surface configurations' – reflecting the existence of a smooth Stokes inversion):

Performance of a quantum sensor for portal monitoring

- Radiation sensors monitor vehicles passing through border crossings, looking for hidden radioactive threats (SNM, assemblies, …)
- Present sensors have difficulty detecting shielded or low radioactive material (e.g. U235)
- Shielding increases the mass of material in a vehicle
- Can quantum sensors of gravitational fields be used to detect shielded material?

Distribution of fissile sources from LLNL unclassified smuggled fissile models

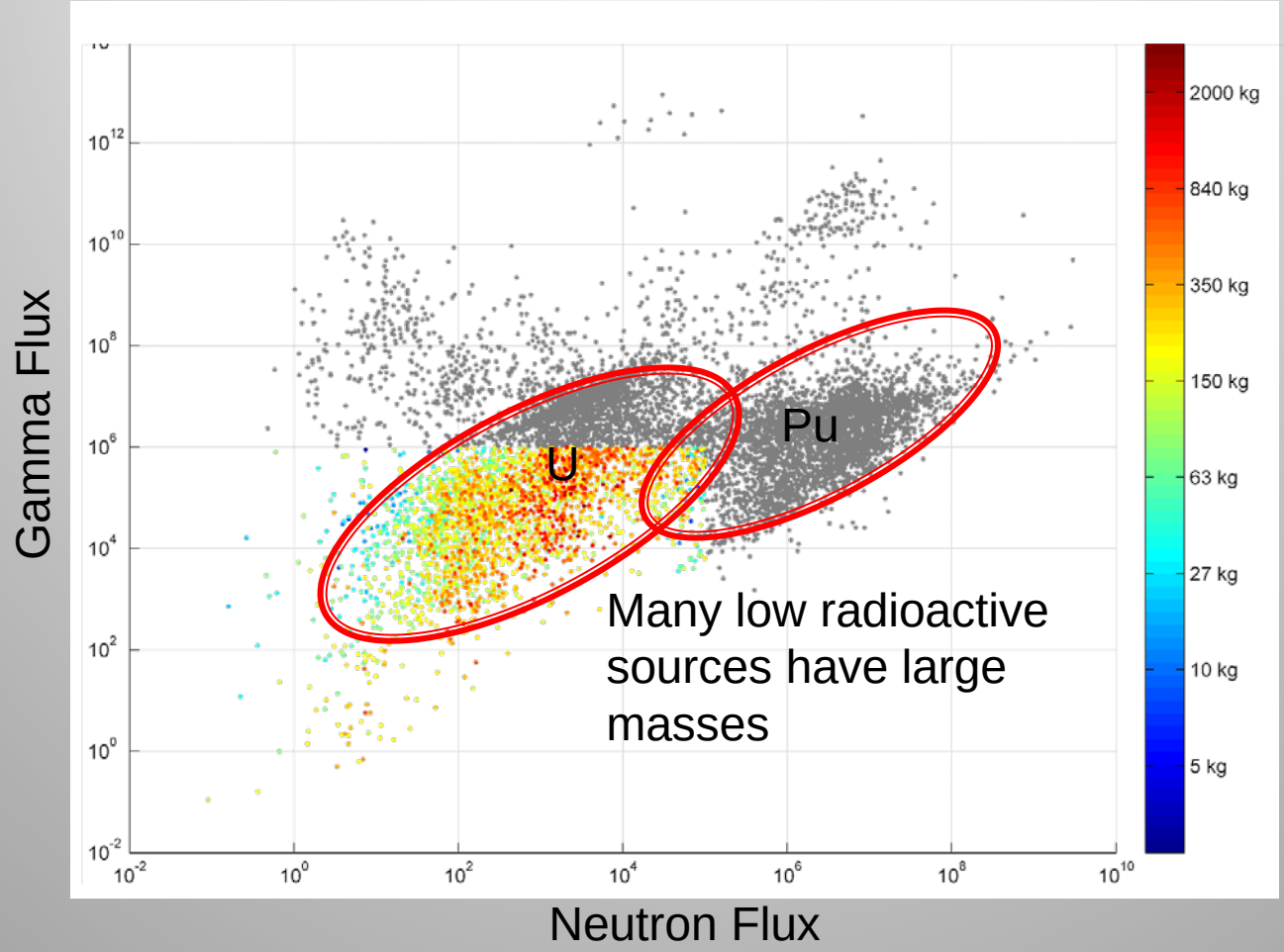

Steps for estimating effectiveness of cold-atom gravimeters for portal monitoring

- Construct sensor model
- Conceptual design of portal system
- Formulate detection algorithm
- Identify design and environmental factors that impact performance
- Design ensemble of experiments (simulated) for Monte Carlo estimation of performance probability distributions (e.g. P_D, P_{FA})
- Perform simulations and calculate performance metrics (ROC curves)

Sensor model: gravimeter response to uniformly moving point mass

- **Gravimeter phase difference $\Delta\varphi$ at position r and launch time *t* is proportional to the gravitational acceleration F_a caused by a point mass with trajectory $r_a(t)$ moving at a constant velocity v_a*:**

$$\Delta\varphi(\mathbf{r},t) = T^2\mathbf{k}_{eff}\cdot\mathbf{F}_a(\mathbf{r}-\mathbf{r}_a(t+T_1+T)+\Delta\mathbf{r}_c) \qquad \mathbf{k}_{eff} = (0,0,k_{eff})$$

$$\Delta\mathbf{r}_c = \Delta\mathbf{v}(T_1+T)+\frac{1}{2}\mathbf{g}(T_1+T)^2+\frac{1}{12}\mathbf{g}T^2$$

$$\Delta\mathbf{v} = \mathbf{v}_0-\mathbf{v}_a\ , \qquad \mathbf{g} = (0,\ 0,\ -9.81\ \mathrm{m}^2/\mathrm{s})$$

v_0: launch velocity, T_1: time to first laser pulse,
T: time between laser pulses

- **Sensor response for one cycle is** $\Delta\varphi(\mathbf{r},t)\ +n_\varphi v, \quad v\sim N(0,1)$

- **Sensor noise is iid Gaussian with rms of n_φ**

***Ref: Alan Zorn, "DNDO Gravity Sensor Measurement Model (Rev 3)," AOSense report, June 15, 2012**

Formulation of detection statistic when signal is uncertain

- Given time series data from N sensors in an array, determine whether a mass went through the array (detection)
- Without knowing the form of a positive detection signal, it is difficult to formulate a detection statistic
- One approach is to construct a noise statistic for a sequence of time windows that measures the probability that the data is only noise in each time window
- Optimal approach for additive Gaussian noise is analysis of variance (ANOVA) to calculate probability that data is noise
- Detection statistic for ANOVA is described by the F distribution with N-1 and N*(K-1) degrees of freedom (N sensors, K samples in time window)
- If the probability of noise drops below a given threshold (say 1%), then we can say that the probability that the data is only noise is <1%, or conversely that the probability of a mass is >99%.

Calculation of detection statistic using windowed ANOVA on simulated data

Probability of noise

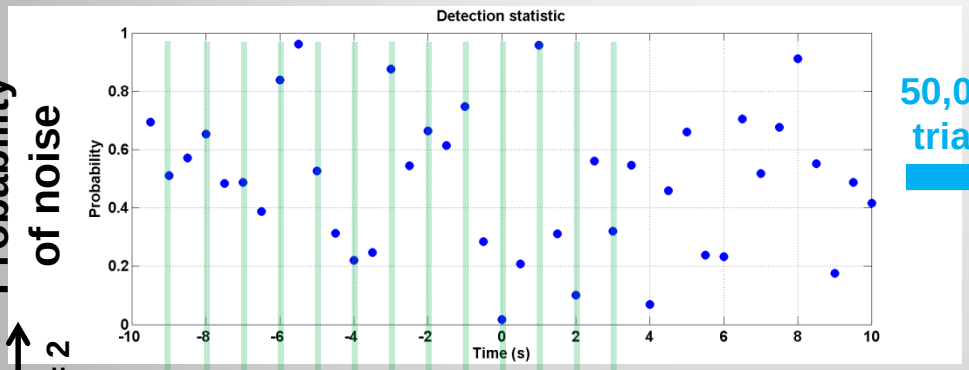

ANOVA

Window size = 2

Data

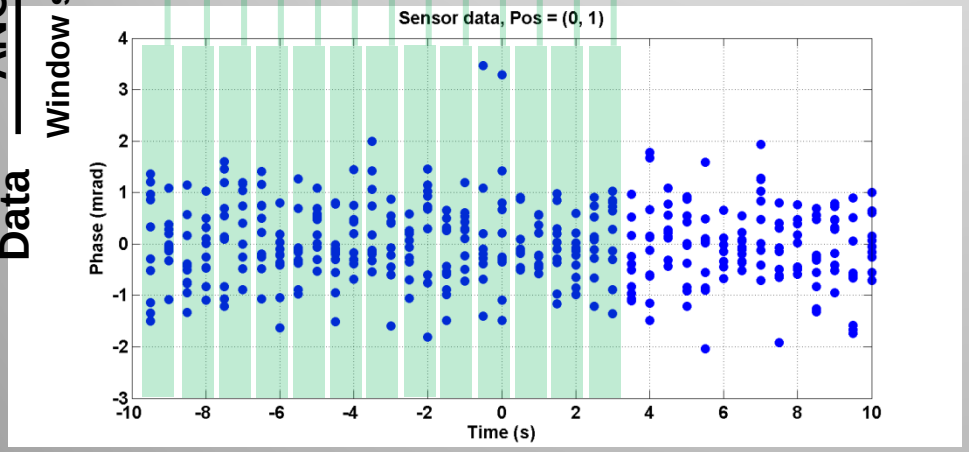

50 kg point mass, 3 MPH, 1 m height

50,000 trials

Cumulative distribution of detection statistic

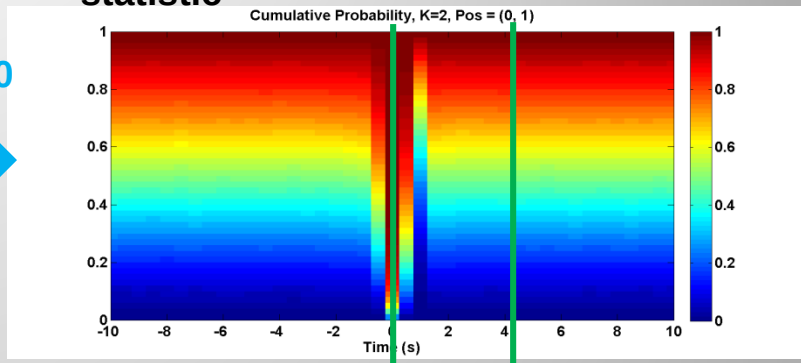

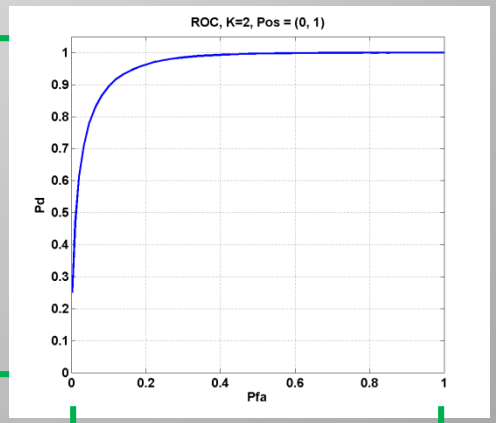

Rectangular array of 10 gravity sensors with Yaris and point mass

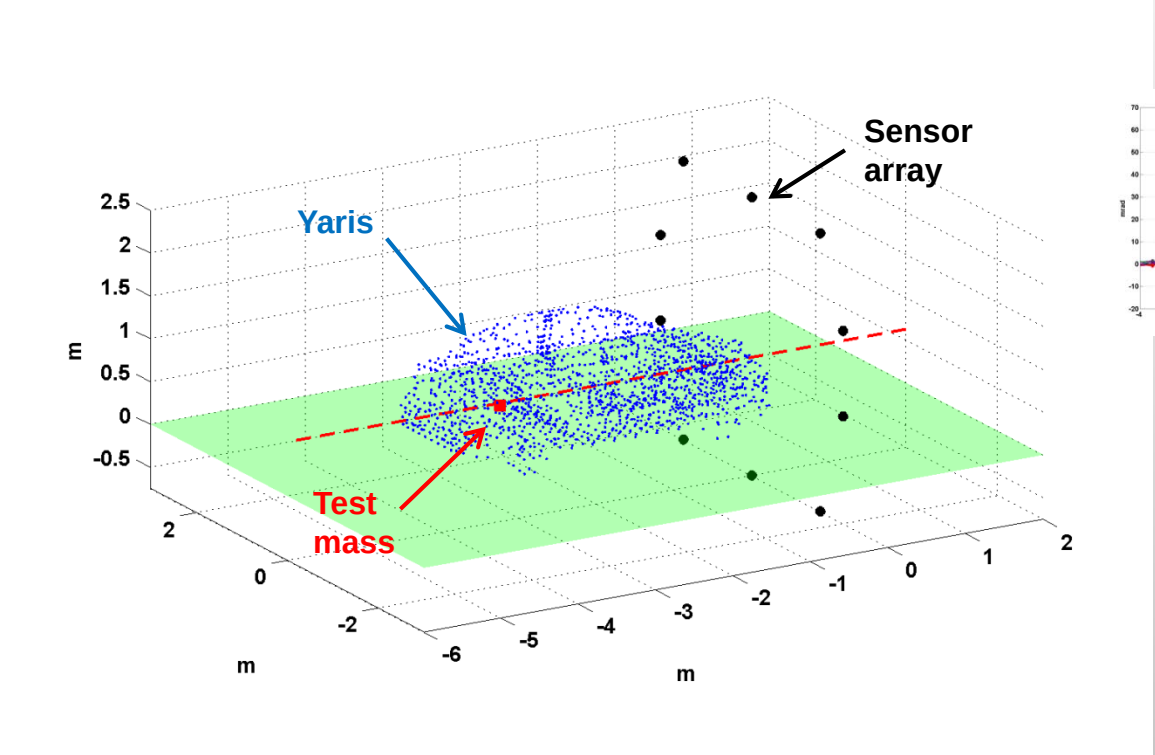

Yaris alone

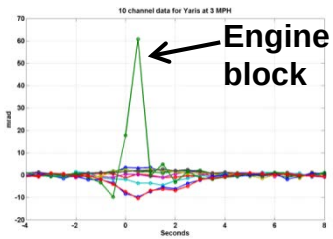

Yaris + mass

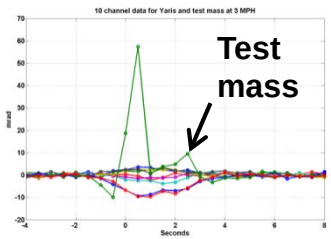

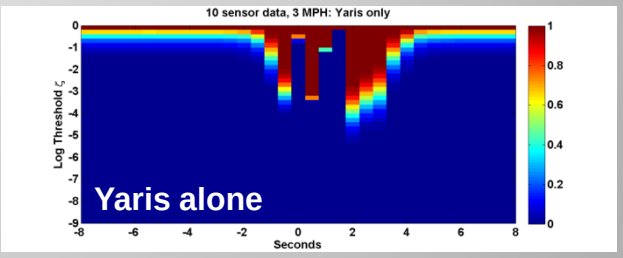

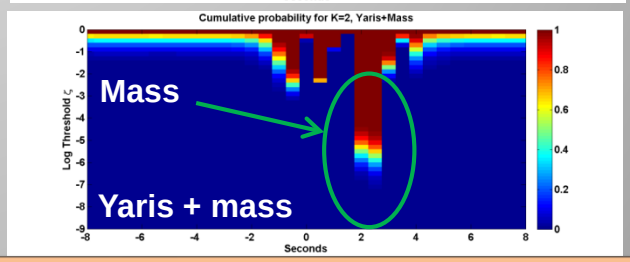

Test mass of 50 kg is placed 0.6 meters above the ground along the mid-plane of a Yaris moving at 3 MPH through a sensor array

Presence of mass clearly modifies sensor response when it is well separated from engine block

Vehicle models from National Crash Analysis Center, George Washington University

Design Variables (12 Factors)

Trajectory				Clutter					Threat		
Vehicle type	X-offset (m)	theta (deg)	tzero (sec)	driver mass (kg)	front passenger mass (kg)	back passenger #1 mass (kg)	back passenger # 2 mass (kg)	back passenger # 3 mass (kg)	threat mass (kg)	threat mass location	threat mass shape (length)
8 vehicles	[-0.75, 0.75] in steps of 0.1	[-3, 3] in steps of 1	[0, 0.49] in steps of 0.05	[50 - 100] uniform RV	0	0	0	0	[50 - 150]	trunk, empty seats in the back or front	spherical or cylindrical
				[50 - 100] uniform RV	[50 - 100] uniform RV	0	0	0			
				[50 - 100] uniform RV	[50 - 100] uniform RV	0	0	[50 - 100] uniform RV			
				[50 - 100] uniform RV	[50 - 100] uniform RV	0	[50 - 100] uniform RV	0			
				[50 - 100] uniform RV	[50 - 100] uniform RV	[50 - 100] uniform RV	0	0			
				[50 - 100] uniform RV	[50 - 100] uniform RV	[50 - 100] uniform RV	0	[50 - 100] uniform RV			

Vehicles: Caravan, F250, Metro, Neon, RAV, Silverado, Taurus, Yaris

Use driver & passenger mass variation as source of "clutter"

Point mass model for medium adult male (81.5 kg)

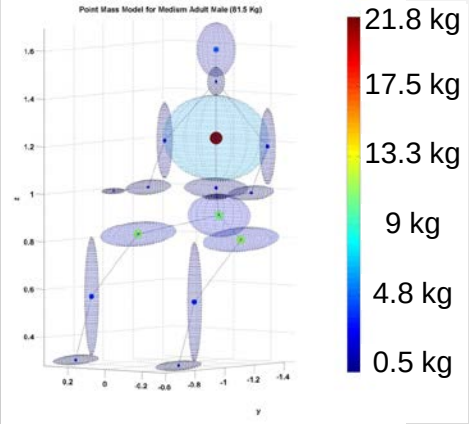

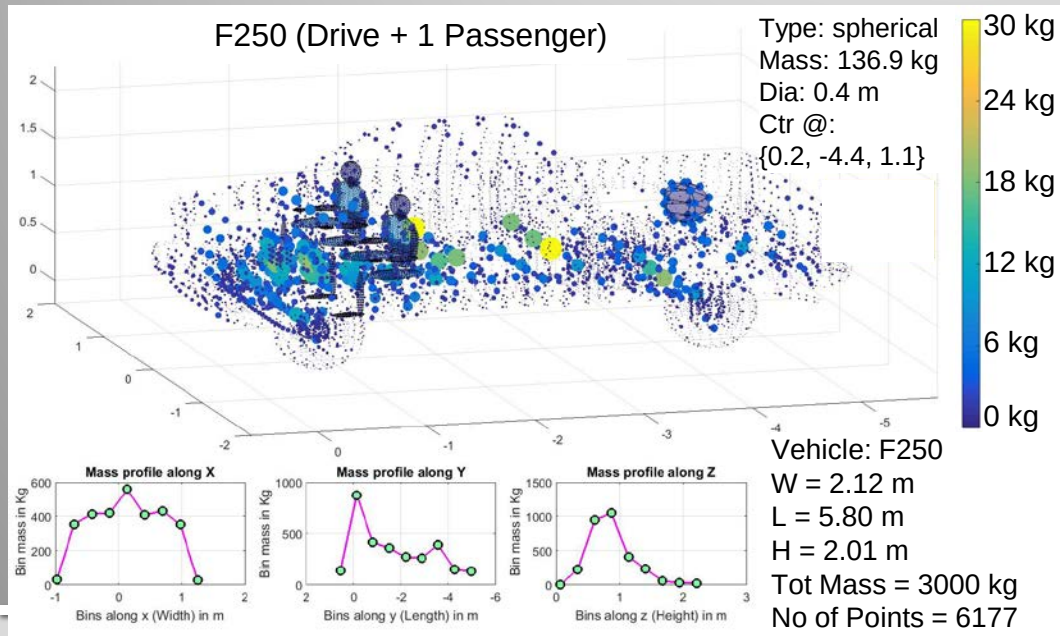

- Based on USAARL Report #88-5 (1988) for male aviators
- Total mass is 81.5 kg (standard)
- For simulated data vary the total mass and point locations by a factor of 0.7 to 1.2, chosen randomly from a uniform distribution
- Assume portal has a vehicle occupancy detector to tag occupant locations.
- Signal consists of contributions from vehicle occupants (clutter) as well as added point mass (signal)
- **Use a Least Squares based approach to model vehicle occupants clutter as a weighted sum of signals due to "Mass man" located in occupant positions.**
- Threat mass from the spanning set is placed wherever geometrically possible (seats, trunk, floor)

Calculating PDFs using vehicle models requires careful experimental design

- Sampling entire parameter space (H0 ~ 2.52 million, H1 ~ 252 million) is not possible in a reasonable computational time
- Requires careful sampling of parameter space to obtain accurate estimates of PDFs
  - Avoid inadvertent concentration of samples in sub-domain of parameter space
- Employ statistical theory of experimental design
  - “Space-filling” designs (Latin hypercube)
  - Reduces sampling to ~24,000 runs

Results: summary of performance over all 8 vehicle types for masses > 50 kg

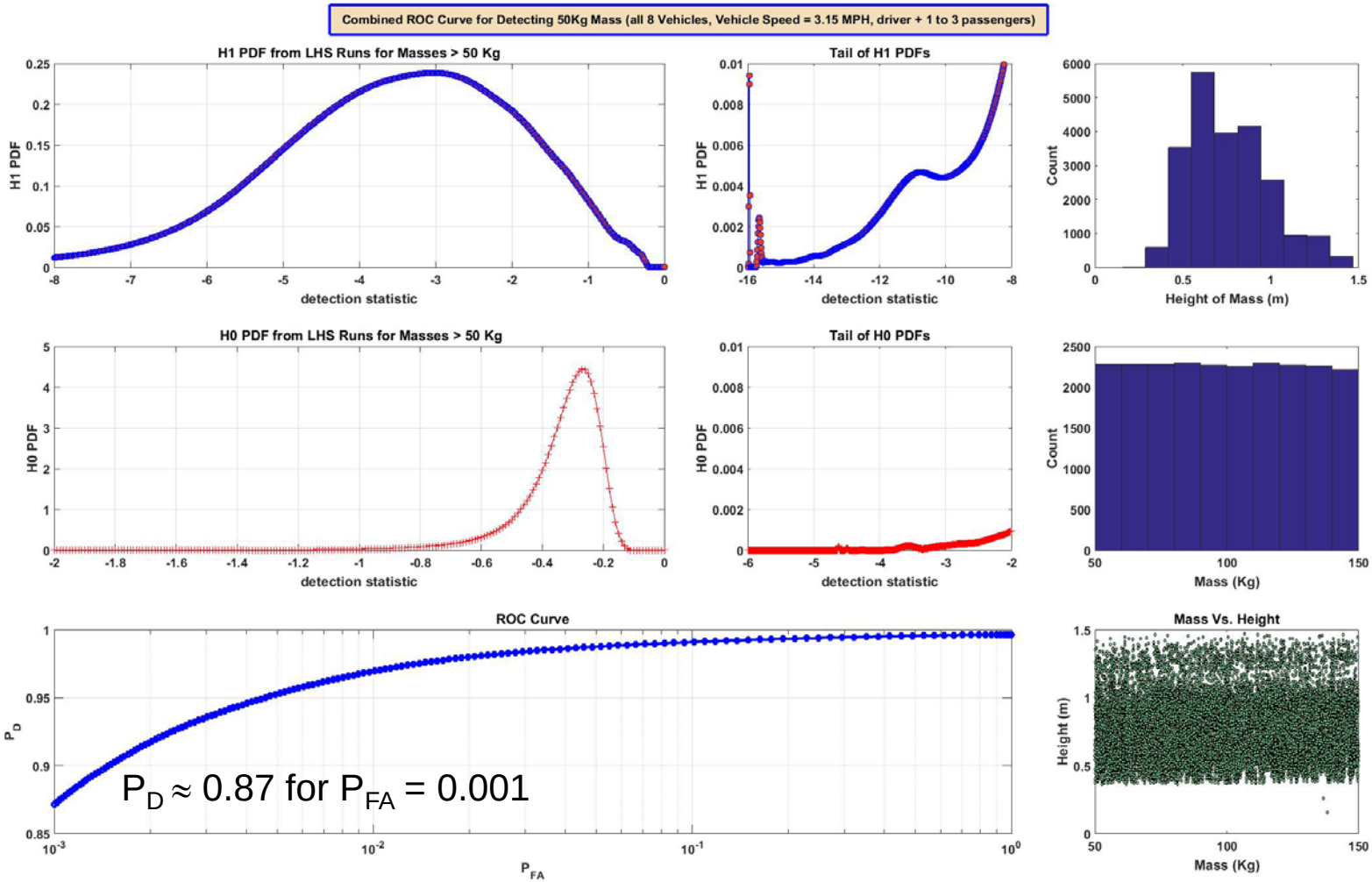

Combining radiation and gravity sensing

Maximizing P_d for a given P_{fa} involves decision trade-offs between radiation and gravity sensing thresholds

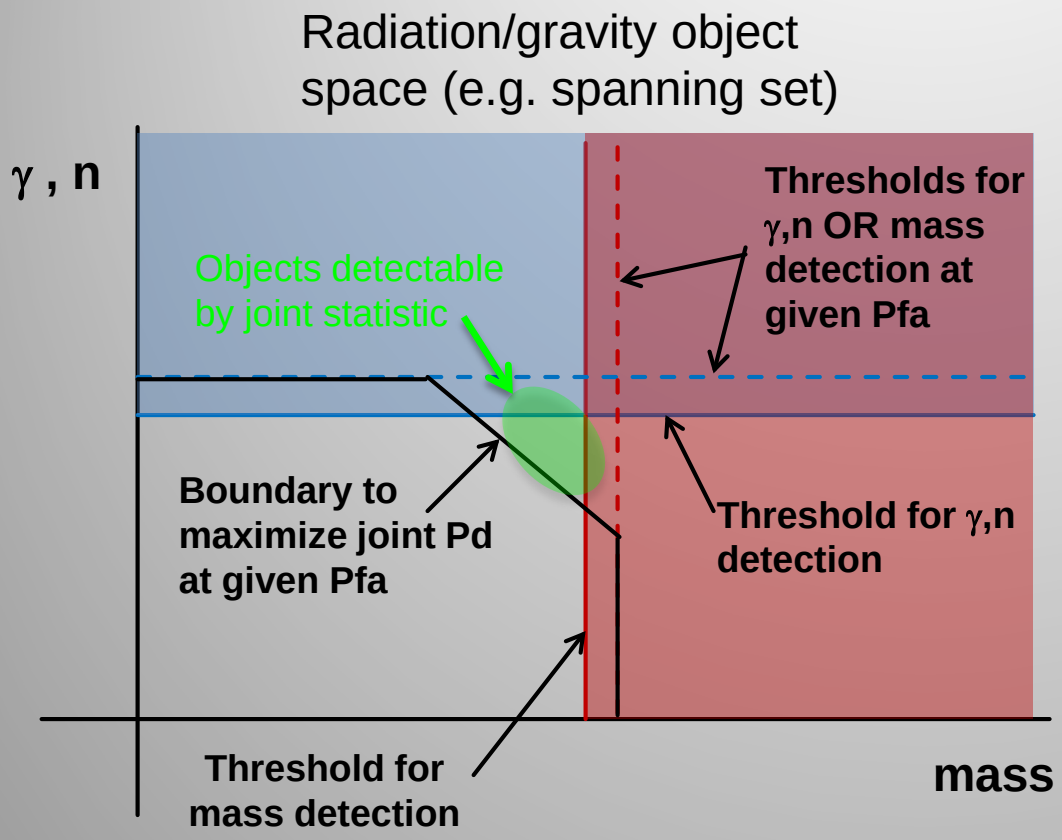

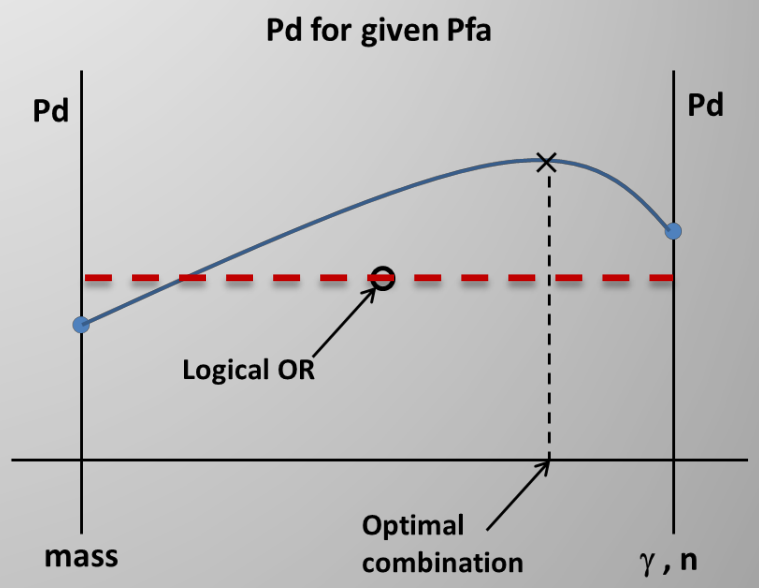

ROC curves and pdfs for 3 radiation sources (low, medium, high)

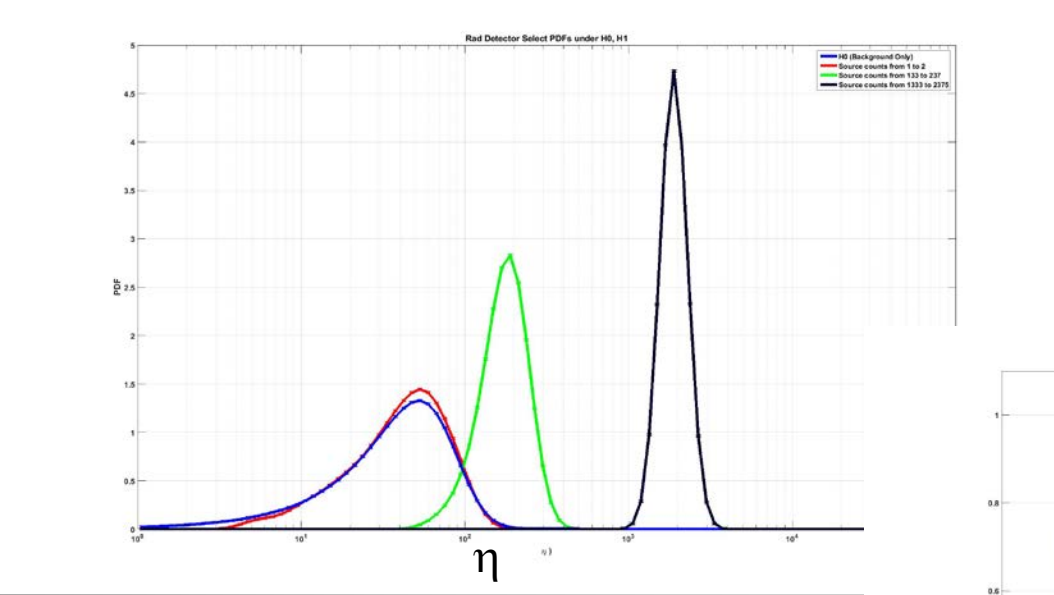

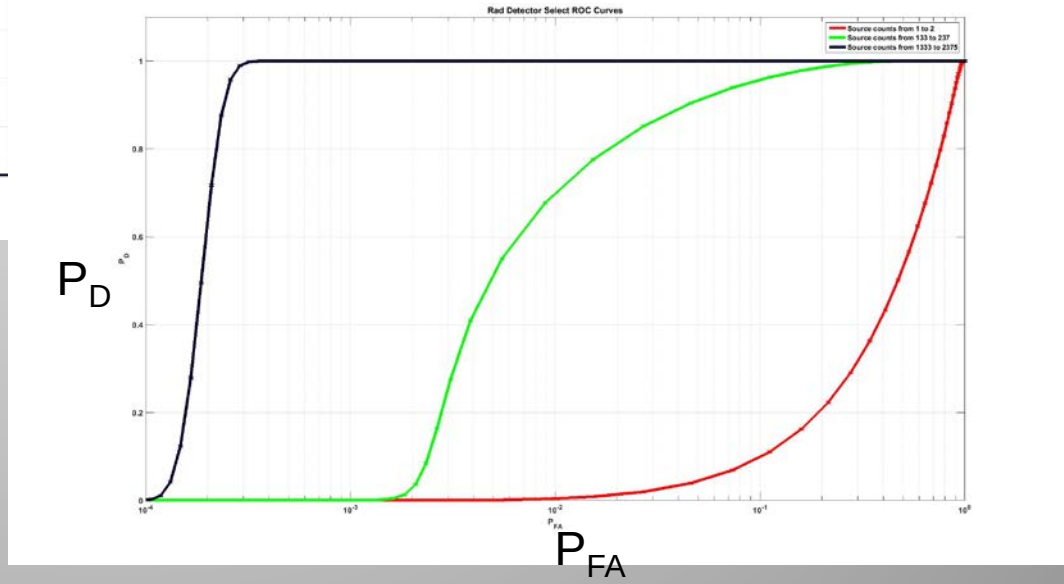

Combining gravity and radiation sensor decisions involves the joint distribution of the mass and radiation detection statistics

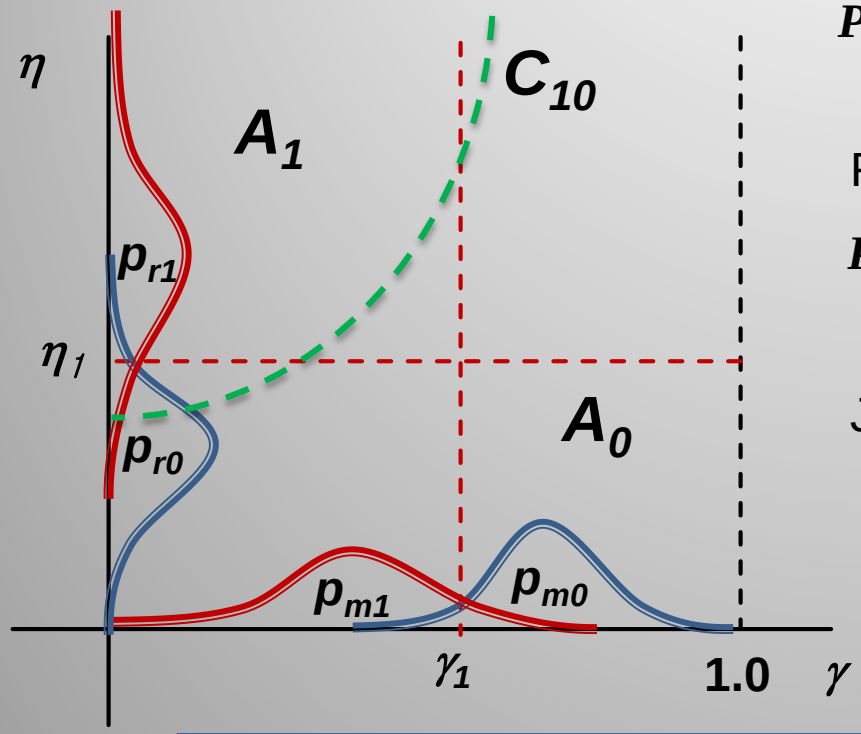

Mass detection

$$P_{FA} = \int_0^{\gamma_1} p_{m0}(\gamma)d\gamma, \;\; P_D(m) = \int_0^{\gamma_1} p_{m1}(\gamma \mid m)d\gamma$$

Radiation detection

$$P_{FA} = \int_{\eta_1}^{\infty} p_{r0}(\eta)d\eta, \;\; P_D(s) = \int_{\eta_1}^{\infty} p_{r1}(\eta \mid s)d\eta$$

Joint mass/radiation detection

$$P_{FA} = \int_{A_1} p_0(\gamma,\eta)d\gamma d\eta\,,$$

$$P_D(m,s) = \int_{A_1} p_1(\gamma,\eta \mid m,s)d\gamma d\eta$$

How do you choose contour C_{10} that maximizes P_D given P_{FA}?

Optimum C_{10} is a contour level of the likelihood function $\Lambda(\gamma,\eta|m,s)$ (Neyman-Pearson)

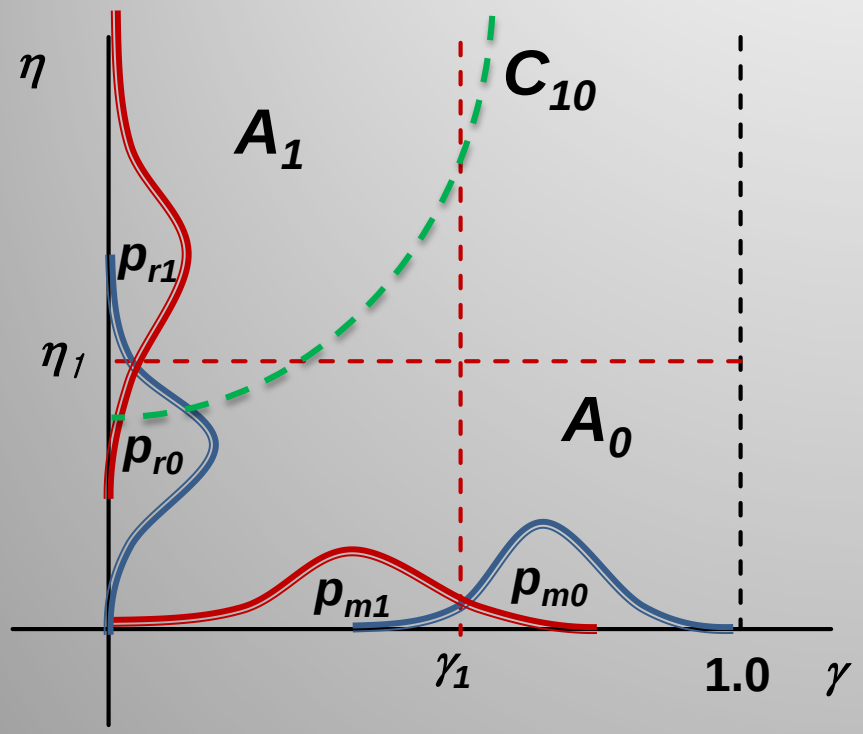

Mass sensor noise and radiation sensor noise are independent

$$p_0(\gamma,\eta) = p_{m0}(\gamma)\,p_{r0}(\eta)\,,$$

$$p_1(\gamma,\eta\,|\,m,s) = p_{m1}(\gamma\,|\,m)\,p_{r1}(\eta\,|\,s)$$

Region A_1 is defined by the condition for the likelihood function

$$\Lambda(\gamma,\eta\,|\,m,s) = \frac{p_{m1}(\gamma\,|\,m)\,p_{r1}(\eta\,|\,s)}{p_{m0}(\gamma)\,p_{r0}(\eta)} \geq \lambda$$

where λ is obtained from

$$P_{FA} = \int_{A_1} p_{m0}(\gamma)\,p_{r0}(\eta)\,d\gamma\,d\eta = C_0$$

C_0 is the desired P_{FA}

Neyman-Pearson decision combination for high mass, low radiation objects

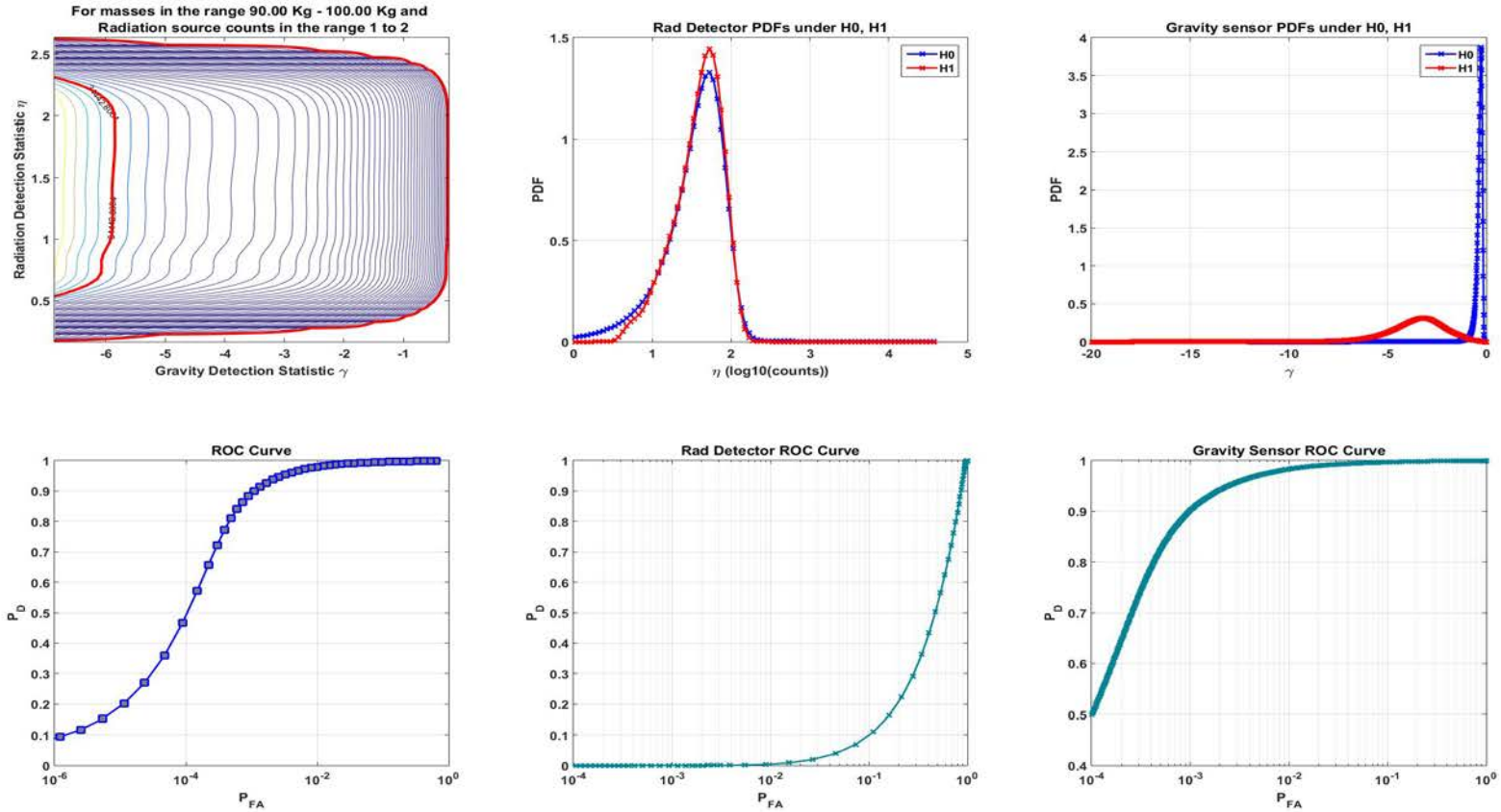

Neyman-Pearson decision combination for low mass, medium radiation objects

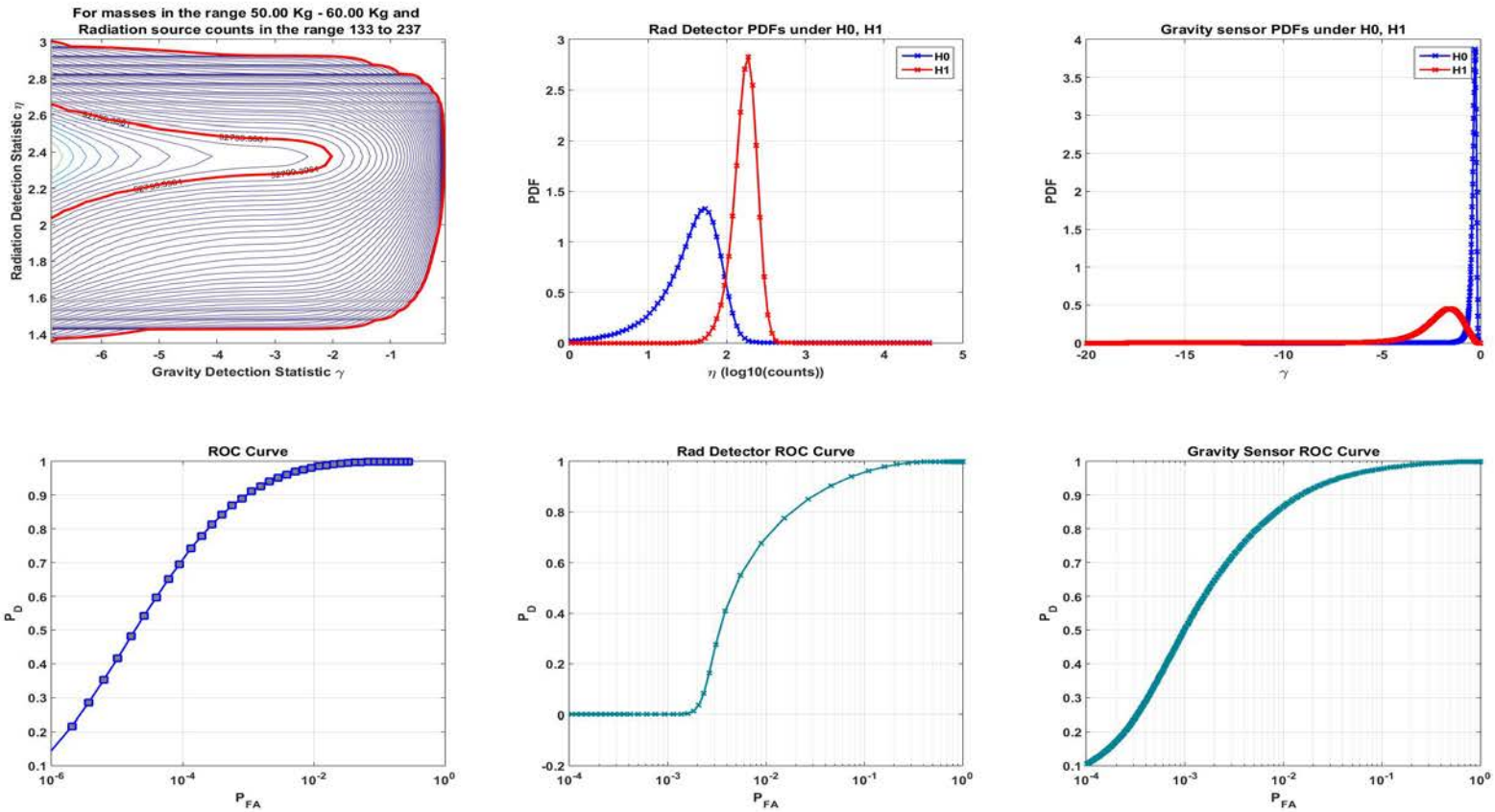

Variation of Pd for a Pfa = 0.001: NP

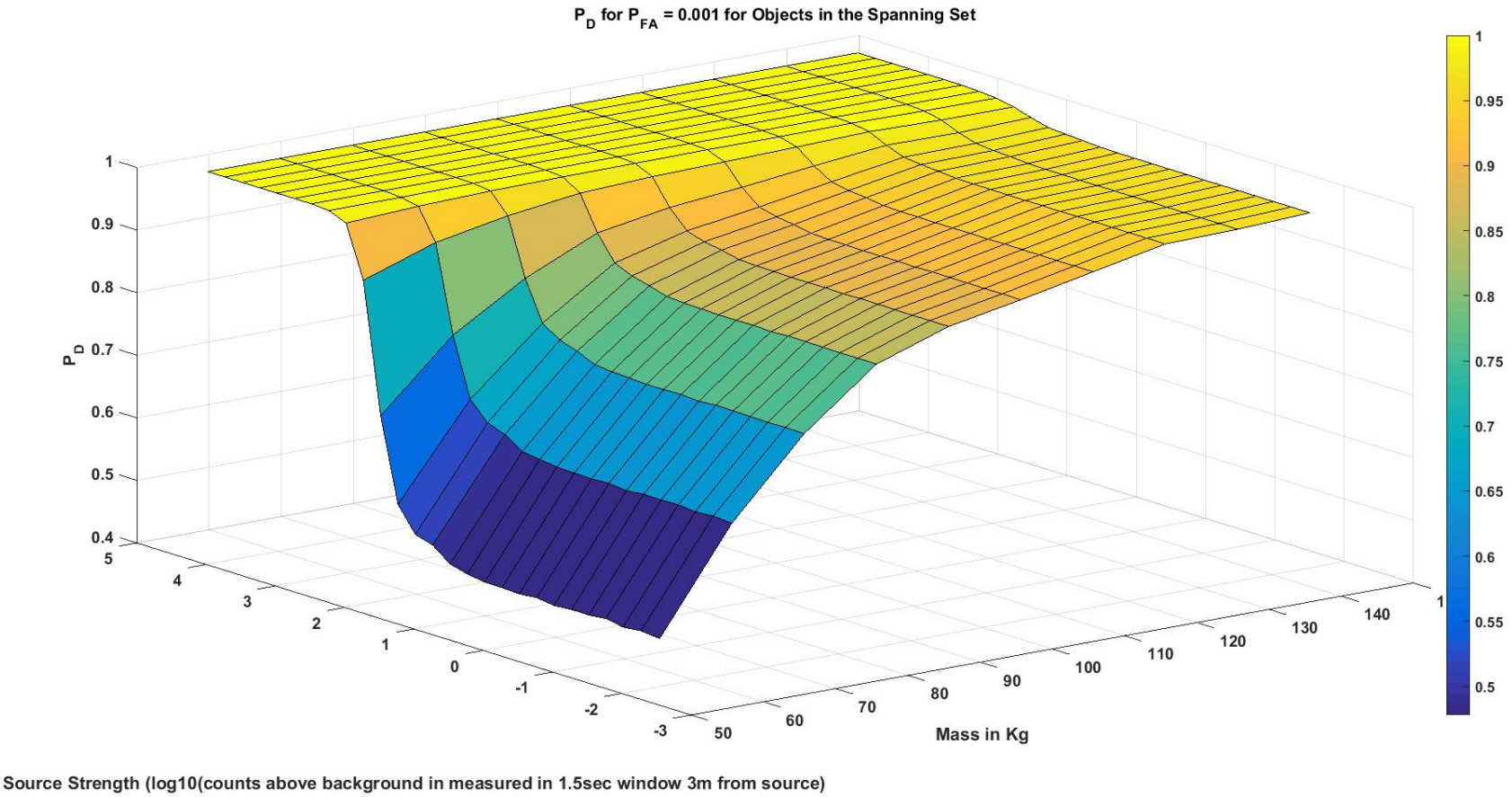

Region of mass/source space for P_{fa} = 0.001

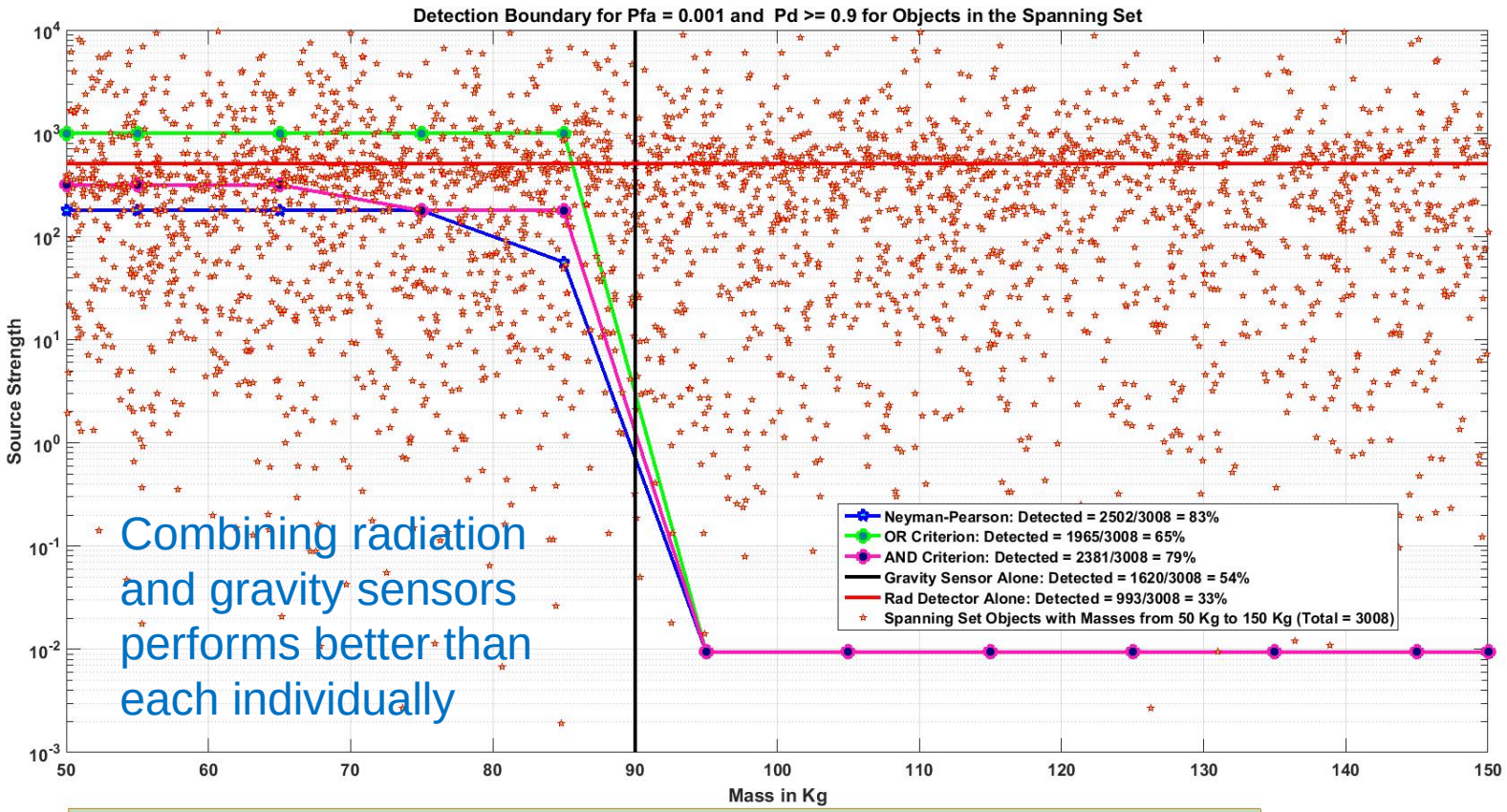

Note: Source strength is measured in counts above background measured over 1 sec window at a distance of 3.5 m from the source

Overall results for P_D and P_C

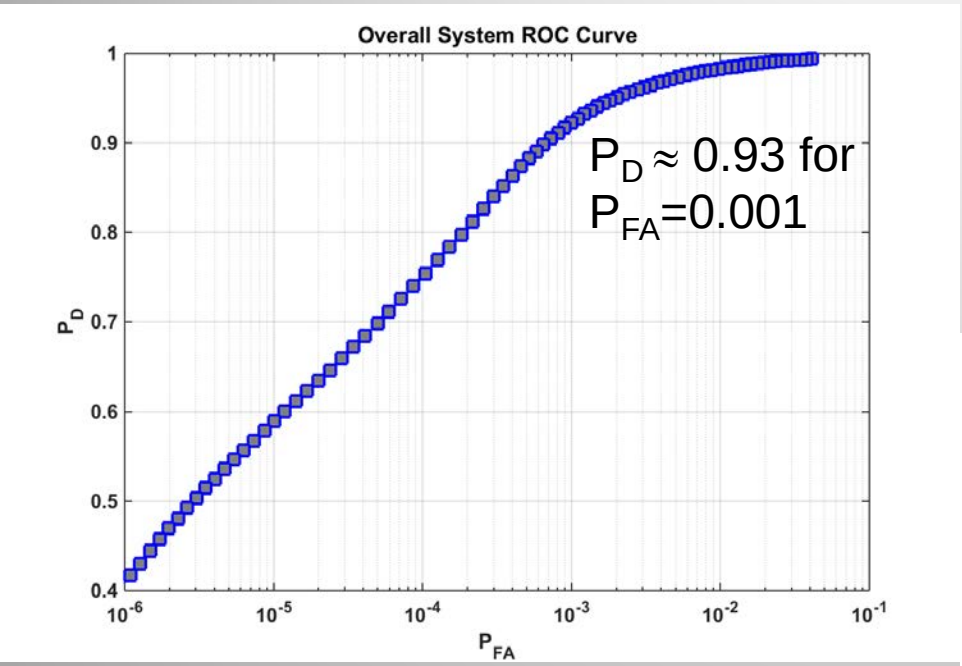

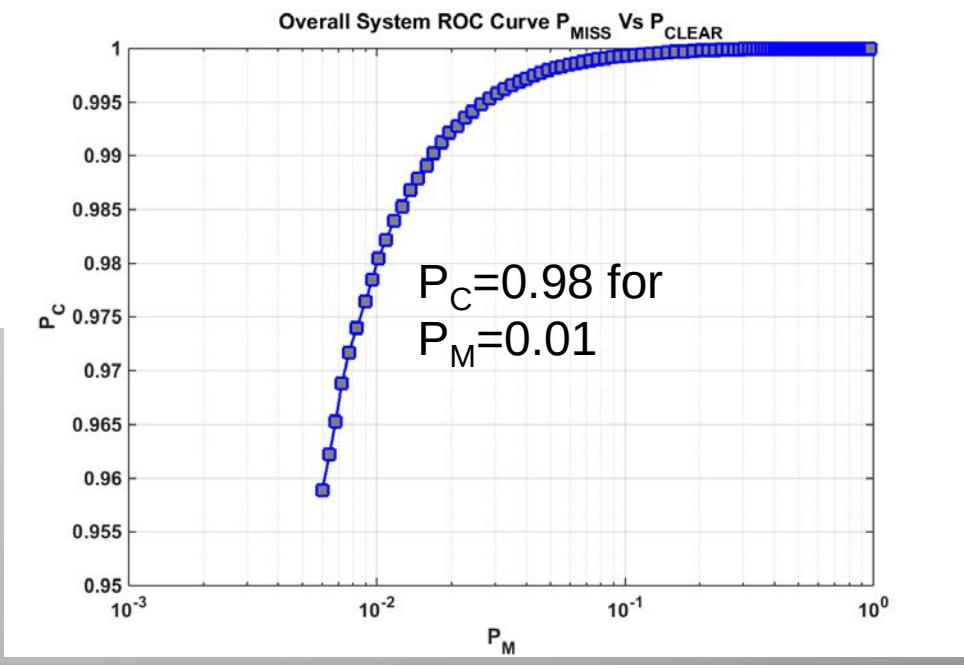

Conclusion

- Cold atom gravity sensors could be useful in detecting shielded threats at a border crossing
- It is possible to estimate the impact of a proposed quantum sensor applied to an important practical problem
- Estimation involved
  - Good models of sensors and sources
  - Solving the detection problem
  - Monte Carlo approach for calculating probability distributions

Acknowledgements

LLNL: Steve Libby, Dave Chambers, Hema Chandrasekaran, Vijay Sonnad, Karl Nelson, Lance Bentley-Tammero, Steve Kreek

AOSense, Inc.: Miro Shverdin, Alan Zorn, Boris Dubetsky, Brent Young

DHS/DNDO TARD project 2012-2015

Backups

Monte Carlo Sampling vs. Latin Hypercube Sampling

Ho:

- Vehicle trajectory parameters: X-offset (-0.75m 0.75m), angle (-3º to +3º), time of portal entry relative to cold atom molasses trajectory (0 to 0.5 sec → divided into 10 intervals) gives 8*7*10 = 560 trajectories
- Passengers: A driver + 1 to 3 passengers → 5 combinations
- Mass of passengers: drawn from a uniform distribution of 56 Kg to 89 kg → 30 Monte Carlo samples

H1:

- For each of the above runs, 50 threat mass objects from cylindrical masses, 50 from spherical masses

Finally add instrument noise (30 Monte Carlo runs) for H0 and H1

For regular Monte Carlo Sampling, total number of runs for H0 = ~2.52 million and for H1 = ~252 million

For LHS, number of MC runs for each iteration = 24,000 (~4 orders of magnitude reduction in computation)

Process Flow of Performance Characterization
How do we get the PDF under H_0 and H_1?

- Vehicle is a collection point masses describing each vehicle
- Clutter is a function of occupants configuration and occupants mass distribution (driver and/or 1 or more (up to 3) passengers with masses drawn from a uniform distribution weights fro 50 Kg to 100 Kg)
- Vehicle trajectory is a function of X-offset, theta, t0 $\rightarrow \Delta x, \Delta\theta, \Delta t_0$
- Sensor geometry is a function of sensor configuration (number and placement of cold atom gravity sensor) and the instrument parameters including noise)
- Threat mass is characterized by its location in the vehicle, its mass, diameter, and or length

Occupants' location in the vehicle

Vehicle speed

H0 = $\mathcal{F}$(vehicle, clutter, trajectory, sensor array geometry)

H0

H1

Sensor array response signal (measurement data)

$\mathbf{y}(t)$

Estimate trajectory (by generating sensor array response templates and Least Squares matching)

$\hat{\Delta x}, \hat{\Delta\theta}, \hat{\Delta t}_0$

Generate array response to vehicle + occupants (using matching template)

$\hat{T}(\hat{\Delta x}, \hat{\Delta\theta}, \hat{\Delta t}_0,$ occupants configuration, occupants masses)

H1 = $\mathcal{G}$(vehicle, clutter, trajectory, sensor array geometry, threat mass)

$\hat{\mathbf{y}}(t) = \mathbf{y}(t) - \hat{T}(\hat{\Delta x}, \hat{\Delta\theta}, \hat{\Delta t}_0)$

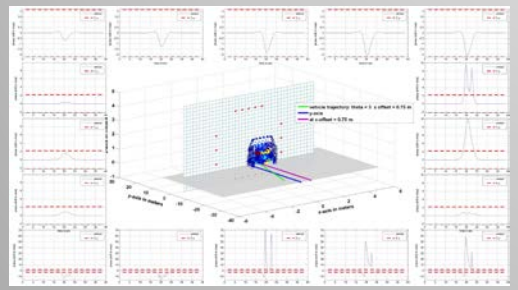

$p(\gamma_{\min}|H_0)$

$p(\gamma_{\min}|H_1)$

Pick minimum detection statistic $\gamma_{\min}$

Windowed ANOVA on residuals (followed by several monotonic transformations)

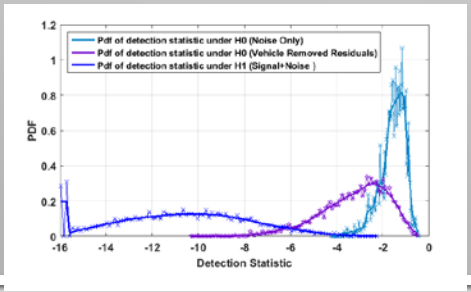

Simulate radiation detection using source injection into vehicle pass-bys from RAIN data

- A Source-detector distance of 3.3 m and vehicle velocity of 10 mph (4.47 m/s) were assumed.
- Set of 8935 1D source models of fissile sources was transported and the detector responses were then calculated (both using GADRAS). The detected count rate at 3.5 m range is used to characterize each source (labeled “s” in pdfs)
- Detector responses were rescaled to represent source-detector encounter parameters and Poisson noise was added.
- Each source profile was then added to a randomly drawn source-free vehicle pass-by and the number of counts within a moving 1.5 sec window was calculated
- The signal (detection statistic) for each pass-by was the maximum window count minus an estimate of the background

Summary for radiation/gravity sensor combination

- Combining radiation and gravity is better than either radiation or gravity alone
- AND combination is better than OR due to lower likelihood of false alarms, allowing lower detection thresholds
- Optimal Neyman-Pearson combination performs best showing 83% of objects detectable at Pfa = 0.001 and Pd>0.9. This increases to 98% for Pfa = 0.01.
- Overall detection performance for the spanning set of test objects achieves Pd = 0.9 for Pfa = 0.001
- Clearance rate of Pc = 0.98 can be achieved if acceptable probability of miss is Pm = 0.01